Applications in Energy and Combustion Science 16 (2023) 100196

Contents lists available at ScienceDirect

Applications in Energy and Combustion Science

journal homepage: www.elsevier.com/locate/jaecs

Data-driven simulation of ammonia combustion using neural ordinary differential equations (NODE)

Manabu Saito *, Jiangkuan Xing, Jun Nagao, Ryoichi Kurose

Department of Mechanical Engineering and Science, Kyoto University, Kyoto daigaku-Katsura, Nishikyo-ku, Kyoto 615-8540, Japan

ARTICLE INFO

Keywords:
Chemical kinetics
Machine learning
Neural ordinary differential equations

ABSTRACT

The direct use of detailed chemical kinetics in combustion simulations is limited by the extremely high computational costs. Recently, Owoyele and Pal (*Energy and AI*, 2022), proposed the neural ordinary differential equations (NODE) method to accelerate calculations of chemical kinetics and proved its effectiveness in zero-dimensional calculations of hydrogen combustion considering 9 species and 21 reactions. However, its performance for more realistic high-dimensional calculations and more complex kinetic systems remains unexplored. Therefore, this study further applies the method for more complex chemical kinetics of ammonia combustion, especially with optimizations in the data sampling, model training strategies, and model application methods that remedy the problems of versatility and application to more practical simulations. The newly developed NODE models are comprehensively validated in the zero-dimensional calculations of ammonia auto-ignition, one-dimensional calculations of laminar freely-propagating ammonia-premixed flames, and two-dimensional direct numerical simulation (DNS) of ammonia-premixed flames in a temporally evolving jet. Present NODE models focus on seven chemical species, namely NH_3, O_2, H_2, OH, H_2O, N_2, and NO, and the results show that, compared with the results obtained by using detailed chemical kinetics, this method is able to reduce the computational costs of the zero-dimensional auto-ignition reaction to 1/24 while reproducing the ignition delay time for a wide range of initial temperatures and equivalence ratios with relatively good accuracy. Additionally, the method is able to reduce the computational costs of the one-dimensional freely propagating flame and two-dimensional jet flame to 1/4 and 1/38 respectively, while acceptable reproduction of the laminar flame speed and temporal evolution of the gas temperature and mass fractions of the interested species can be achieved.

1. Introduction

Numerical simulations for combustion with direct use of detailed chemical kinetics that consider a large number of chemical species and reactions can be computationally expensive when there are significant differences in the time scales of the reactions [1]. For example, while the reaction mechanism of hydrogen combustion proposed by Conaire et al. [2] has the order of 10 species and 20 reactions, the reaction mechanisms of ammonia (NH_3), which is considered one of the next-generation fuels [3], or methane (CH_4) [4] has over 50 species and hundreds of reactions, and to simulate the reactions stably, small time steps must be employed. Therefore, when dealing with the combustion of fuels with such complex chemical kinetics, it is common to use reduced chemical kinetics that only consider a handful of reactions in order to reduce the computational costs [5] or use tabulated chemistry such as flamelet models [6].

In recent years, various calculation methods have been proposed to replace the conventional calculation of the reaction rates of each chemical species using the Arrhenius equation with machine learning, in order to reduce the computational costs while maintaining the generality to apply the method to a variety of conditions. For example, several researchers [7–9] utilized an artificial neural network (ANN) to store flamelet library that exceeds the memory capacity of a general computer while successfully reproducing the result using the conventional flamelet model. Also, the utilization of ANN to predict the reaction rates from the thermochemical states with high precision and generality to solve the stiffness problems in chemical reaction calculations are investigated for fuels such as hydrogen and syngas [10,11]. The output of ANN is often the source terms of the mass fraction of the species, since when a specific time integration procedure is required, the source terms are more convenient and accurate to use in the time integration of mass fractions compared to the directly predicted mass fractions in a fixed time step, which would require interpolations to estimate the source terms.

* Corresponding author.
E-mail address: saito.manabu.63z@st.kyoto-u.ac.jp (M. Saito).

https://doi.org/10.1016/j.jaecs.2023.100196
Received 3 April 2023; Received in revised form 21 August 2023; Accepted 27 August 2023
Available online 2 September 2023

Another example that is recently developed is the method of reducing the computational costs of the reaction rate calculation by applying the neural ordinary differential equations (NODE) [12]. NODE is a computational method that uses a neural network as an ODE solver and directly learns and predicts the derivatives of the ODE. Therefore, when applied to combustion simulations, it is possible to predict the reaction rates in chemical reaction calculation without depending on the time interval, and it is easy to be applied to combustion simulations with various time scales. Owoyele and Pal [13] successfully used NODE to learn and predict the reaction rates of the species and temperature in hydrogen combustion, reducing the computational costs and accurately reproducing the zero-dimensional auto-ignition reaction. However, the applicability of the same method to more complex chemical kinetics with a larger number of chemical species and elementary reactions, such as NH_3 or CH_4 combustion, and higher dimensional calculations (one-, two- or three-dimensional calculations) have not been fully investigated.

Therefore, this study proposes a method that can be applied to chemical reaction calculations with more complex chemical kinetics, based on the chemical reaction calculation method using NODE that Owoyele and Pal [13] conducted, and its effectiveness on calculations for different dimensions is verified. Specifically, the chemical reaction calculation method using NODE is applied to numerical simulations of NH_3 combustion (zero-dimensional auto-ignition reaction, one-dimensional freely propagating flame, and two-dimensional temporary evolving planar jet flame). The ignition delay time, laminar burning velocity, temperature, and mass fraction distribution of various chemical species, as well as the computational efficiency, are compared with the chemical reaction calculation using detailed chemical kinetics, to verify the ability of this method.

2. Numerical methods

To investigate the accuracy of the chemical reaction calculation method using NODE, direct numerical simulations (DNS) employing the conventional detailed chemical kinetics [14] and NODE are performed and compared.

2.1. Governing equations

The governing equations for conservation of mass, momentum, mass fraction of chemical species, and energy are written as

$$\frac{\partial \rho}{\partial t} + \nabla \cdot (\rho \boldsymbol{u}) = 0, \tag{1}$$

$$\frac{\partial \rho \boldsymbol{u}}{\partial t} + \nabla \cdot (\rho \boldsymbol{u}\boldsymbol{u}) = -\nabla p + \nabla \cdot \boldsymbol{\tau}, \tag{2}$$

$$\frac{\partial \rho Y_k}{\partial t} + \nabla \cdot (\rho Y_k \boldsymbol{u}) = -\nabla \cdot (\rho \boldsymbol{V_k} Y_k) + \rho \dot{\omega}_k, \tag{3}$$

$$\frac{\partial \rho h}{\partial t} + \nabla \cdot (\rho h \boldsymbol{u}) = \nabla \cdot \left[\rho D_h \left\{ \nabla h - \sum_k \left(h_k \nabla Y_k \right) \right\} - \rho \sum_k \left(h_k Y_k \boldsymbol{V_k} \right) \right] + \frac{\partial p}{\partial t} + \boldsymbol{u} \cdot \nabla p + \tau : \nabla \boldsymbol{u}, \tag{4}$$

where ρ is the density, $\boldsymbol{u}$ is the velocity, p is the pressure, $\boldsymbol{\tau}$ is the viscous stress tensor, h is the enthalpy, D_h is the diffusion coefficient of heat, h_k is the enthalpy of species k, Y_k is the mass fraction of species k, $\boldsymbol{V_k}$ is the diffusion velocity of species k, and $\dot{\omega}_k$ is the reaction rate of species k. $\boldsymbol{V_k}$ is calculated from the following Stefan-Maxwell equation:

$$\nabla X_k = \sum_{j \neq k} \left\{ \frac{X_j X_k}{D_{jk}} \left(\boldsymbol{V_j} - \boldsymbol{V_k} \right) \right\}, \tag{5}$$

where X_k is the mole fraction of species k, and D_{jk} is the binary mass diffusion coefficient of species k into species j. The calculation of $\dot{\omega}_k$ considers the detailed chemical kinetics of 59 species and 356 reactions proposed by Okafor et al. [14] for NH_3/CH_4 combustion.

2.2. Chemical kinetics calculation using NODE

In this study, first, zero-dimensional auto-ignition calculations of NH_3 are calculated using detailed chemical kinetics for multiple initial temperatures and equivalence ratios, and the training data of the reaction rates with respect to temperature and mass fraction of chemical species is created. Then, NODE is trained from the data to reproduce the reaction rates in chemical reaction calculations.

2.2.1. Training data generation

The training data is generated by chemical reaction calculation using detailed chemical kinetics through Cantera [15]. The reaction rate of the mass fraction, $\dot{\omega}$, is calculated using the following equation.

$$\frac{dY^n}{dt} = \frac{\dot{\omega}^n(Y^n, T^n; t)}{\rho}, \tag{6}$$

where $\dot{\omega}$ is calculated using the Arrhenius equation, and it is implicitly time integrated by Variable-coefficient ODE (VODE) [16]. Furthermore, since the time scales for auto-ignition calculation for each initial condition are different, using a constant time step dt for all conditions results in an imbalance in the number of data for each condition. In order to train NODE accurately, it is necessary to prevent the imbalances in the number of data among conditions. A straightforward solution would be to make the number of data equal for each condition. Thus, the number of data generated for each initial condition is defined as N, and the time step dt and elapsed time t_{elap} are defined using the ignition delay time τ_{ign} as follows.

$$dt = 4 \times \frac{\tau_{\mathrm{ign}}}{N} \tag{7}$$

$$t_{\mathrm{elap}} = 4 \times \tau_{\mathrm{ign}} \tag{8}$$

Here, the elapsed time t_{elap} is four times the ignition delay time so that sufficient time is taken for the reaction to become an equilibrium state after ignition. In this study, the training data consists of equivalence ratios of 0.6 to 1.4 with intervals of 0.2 and temperatures of 1500 K to 2300 K with 200 K intervals. Each initial condition consists of N = 10,000 points. The time step is different among initial conditions but fixed in each training data for ease to balance the number of data.

2.2.2. Multi-scale sampling method

In the generation of the training data, while the number of data for each initial condition is kept constant, if random sampling from the training data is performed for each initial condition during NODE training, data whose reaction rate is closer to 0 are sampled at high frequency. For example, Fig. 2.1 shows the reaction rate of the mass fraction of NH_3 with respect to the mass fraction of NH_3 for the training data at an initial temperature of 2100 K and an equivalence ratio of 0.6. From this figure, it is apparent that the data distribution density is higher when the mass fraction of NH_3 is around 0 and 0.09. Therefore, if random sampling from the training data of this initial condition is performed, the data with a higher data distribution density of Y_{NH_3} around 0 and 0.09 will be more frequently sampled than the data with lower data distribution density. In addition to that, the sampling of data near 0.05 of Y_{NH_3} may not be sufficient, and the prediction accuracy in this region may be poor. This issue with the training data distribution was also discussed by Zhang et al. [10] to investigate its effect on prediction accuracy. It was concluded that randomly generating the training data without any consideration of the training data distribution had a negative effect on the prediction accuracy of the reaction rate, and a method to balance the data distribution was necessary. Therefore, in this study, instead of randomly sampling the data in the training process, each data is weighed based on their data distribution density

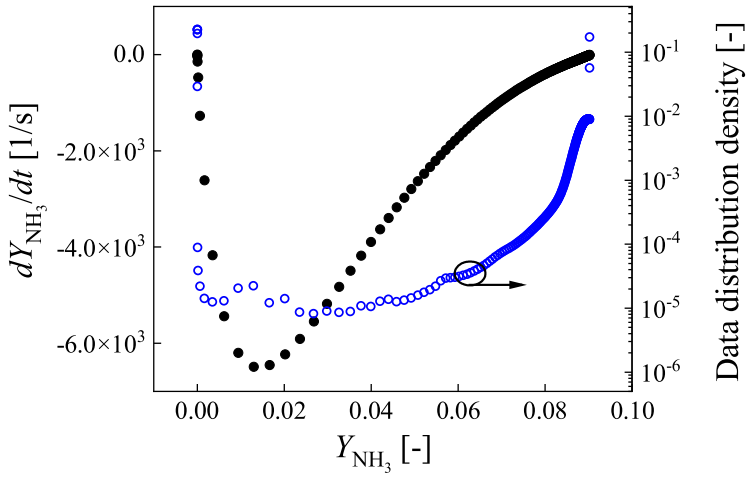

Fig. 2.1. Data distribution of mass fraction versus reaction rate of NH_3 and data distribution density (ϕ = 0.6, T_{init} = 2100 K, plotted every 40 points).

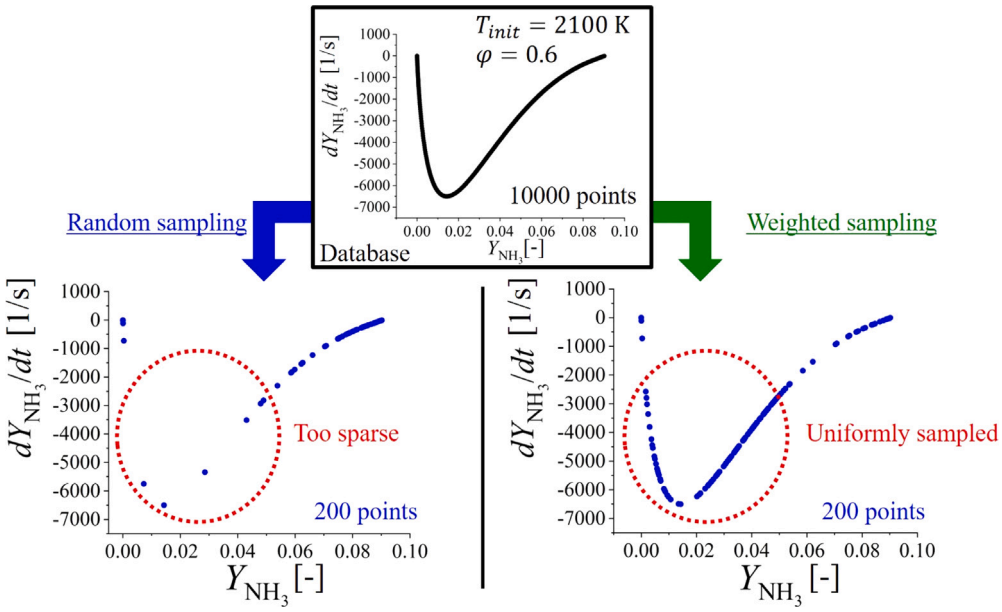

Fig. 2.2. Comparison of sampled data distribution between random sampling and weighted sampling.

and the sampling frequency is adjusted to ensure that the data in low-density regions are sufficiently taken into account. The weight value Q for each data is defined the following,

$$Q = \frac{P_{\min}}{P} \tag{9}$$

where P is the data distribution density obtained by kernel density estimation that estimates the probability density, and $P_{\min}$ is the minimum value of P in the entire training data. As a result, by comparing the data distribution of the 300 points that are randomly sampled with that sampled with weighting using Q shown in Eq. (9), it can be clearly seen that when weighting is applied using Q, a better sampling can be observed in the region of $0 \leq Y_{NH_3} \leq 0.05$ compared with randomly sampled ones. This enables NODE to be trained uniformly across the entire training data, leading to improvement in the accuracy of NODE prediction (see Fig. 2.2).

2.2.3. Normalization

Mass fractions of species are normalized using customized Box–Cox transformation (BCT) [17], which is defined as

$$f(x) = \begin{cases} \frac{x^{\lambda}-1}{\lambda} & \text{(consumption species)} \\ \frac{(1-x)^{\lambda}-1}{\lambda} & \text{(production species)} \end{cases}, \tag{10}$$

where λ is set as 0.1, the consumption species are NH_3 and O_2, and the production species are the rest. The transformation has two options, and this is to avoid a significant increase in the transformed mass fraction of the production species when their original mass fractions are close to zero. For temperatures, it is normalized by simply dividing by the maximum value in the entire training data.

2.2.4. Training

The generated training data and the sampling method are used to train NODE. Fig. 2.3 shows the schematic of the training procedure. The input of NODE is the mass fraction of each chemical species and temperature, and the output is the reaction rate of one of the

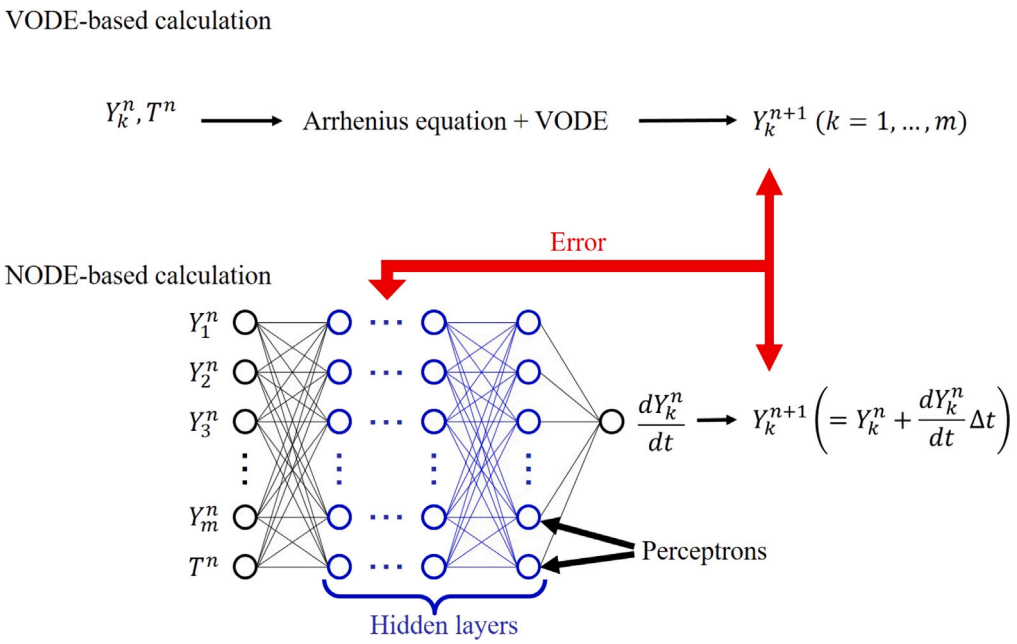

Fig. 2.3. Schematic of the training procedure of NODE.

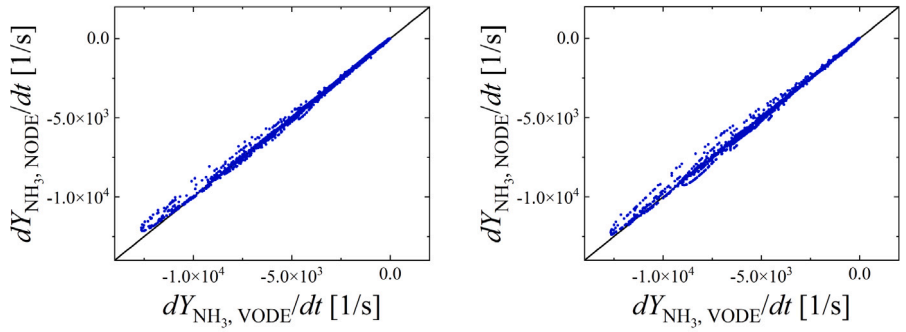

Fig. 2.4. Comparison of reaction rate prediction of NH_3 using NODE and VODE between species selection threshold of 1.0×10^{-2} and 1.0×10^{-3}.

chemical species. Therefore, chemical reaction calculation using NODE is represented as follows, and each chemical species is introduced separately using NODE.

$$\frac{dY_k^{n+1}}{dt} = \frac{\dot{\omega}^n(Y_k^n, T^n; t)}{\rho} \tag{11}$$

Here, Y^n and T^n denote the mass fraction and temperature of the chemical species considered in NODE, respectively. The mass fraction of each chemical species used as input to NODE does not consider all of the chemical species involved in the detailed chemical kinetics, but only the mass fraction of the chemical species whose maximum value of mass fraction in the training data exceeds a threshold. This is because the use of all chemical species considered in the detailed chemical kinetics as inputs to NODE results in the complexification of the neural network used in NODE and an increase in computational costs due to the enlargement of the number of parameters. In this study, the threshold is set to 1.0×10^{-2}, and as a result, the chemical species used as inputs to NODE are seven species, namely NH_3, O_2, H_2, OH, H_2O, N_2, and NO. Additionally, the calculation for the mass fraction of N_2, which is an inert chemical species, is excluded from NODE, and it is calculated by subtracting the mass fractions of the remaining species from one. Therefore, 6 NODEs are considered to calculate the reaction rates for NH_3, O_2, H_2, OH, H_2O, and NO.

As a preliminary analysis conducted prior to one- and two-dimensional calculations, the threshold is lowered from 1.0×10^{-2} to 1.0×10^{-3} to test the influence of the number of considered species on the calculation results. Additional chemical species are considered, which are H, O, NH, NH_2, N_2O, and N_2H_2, and the effect of the threshold on the prediction accuracy is investigated. Figs. 2.4(a) and 2.4(b) show the comparisons of predicted reaction rates obtained using NODE with ground truth reaction rates obtained using VODE for NH_3 under the same sampling condition as the training data. The sampled data are 40,000 in total. From these figures, it can be observed that the reaction rates obtained using NODE have a good correlation with those obtained using VODE in both of the thresholds, and they are almost identical, indicating that the threshold difference between 1.0×10^{-2} to 1.0×10^{-3} has very little influence on the prediction accuracy.

Next, Fig. 2.5 shows the NODE perturbation test for variations of initial conditions with the species selection threshold of 1.0×10^{-2}. The thermochemical initial conditions for the calculations of auto-ignition are randomly sampled from temperatures of 1900 K to 2300 K, and equivalence ratios of 0.6 to 1.4 for 20 cases. Then, auto-ignition calculations are conducted using those initial conditions by VODE, and for 40,000 thermochemical states in the auto-ignition calculations, the reaction rate predictions obtained by NODE are compared with those obtained by VODE. It can be seen that NODE is capable of reproducing

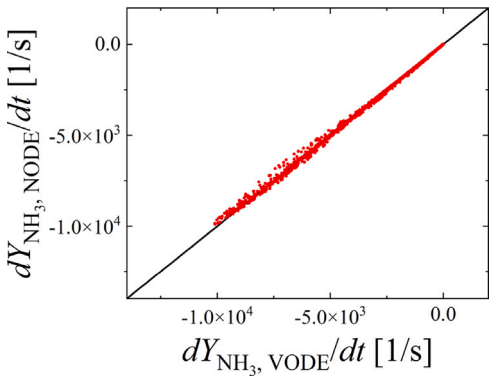

Fig. 2.5. NODE perturbation test.

the reaction rates under perturbated inputs with good accuracy. NODE is trained for each chemical species with hidden layers consisting of four layers and each comprised of 32 perceptrons for major species (NH_3, O_2, H_2O), and 64 perceptrons for minor species (H_2, OH, NO). All the different NODEs for each species are trained separately, and while training NODE for one species, the ground truth mass fraction of the other species and temperatures are used as inputs.

For the activation function, sigmoid-weighted linear unit (SiLU) [18] is used in each layer. Also, Fig. 2.6 is the result of the hyperparameter test conducted for NODE of NH_3 and T_{init} from 1900 K to 2300 K as an example. The correlation coefficient indicates the linear correlation of the reaction rates obtained from NODE and the conventional VODE with detailed chemical kinetics, and Fig. 2.6(a) shows its values with the increase in the number of perceptrons when the number of hidden layers is four. From this figure, the prediction accuracy of NODE saturates when the number of perceptrons is 16 and above. Also, Fig. 2.6(b) shows the correlation coefficient with the increase in the number of hidden layers when the number of perceptrons is 32. From this figure, the prediction accuracy saturates when the number of hidden layers is four and above. Therefore, the number of perceptrons and hidden layers in NODE for NH_3 and T_{init} from 1900 K to 2300 K is enough for the saturation of prediction accuracy. This is the same for other major species (O_2 and H_2O), but not for minor species (H_2, OH, and NO), and 64 perceptrons are required to reach the saturation in prediction accuracy. NODEs for minor species have 64 perceptrons for each hidden layer, and this treatment for minor species indicates that a larger model size is required for better prediction accuracy. It also indicates that the reaction rate predictions for minor species are more difficult for NODE than those for major species.

In this study, NODE for each chemical species is branched into three models based on the initial temperature of the training data, predominantly to increase the computational efficiency while maintaining the prediction accuracy. The highest initial temperature model is trained using initial temperatures of 1900 K, 2100 K, and 2300 K. The medium initial temperature model is trained using initial temperatures of 1500 K, 1700 K, and 1900 K. The lowest initial temperature model is trained using initial temperatures of 900 K, 1100 K, 1300 K, and 1500 K. As for the lowest initial temperature model, training data for the initial temperatures of 900 K and 1100 K contains the beginning 5 s of the auto-ignition calculation. This is due to the insanely long ignition delay time that if dt described in Eq. (7) is used, it would result in too large time steps compared with the time step used in the later explained one- and two-dimensional freely propagating flame and temporary evolving planar jet flame. This also means that the training data for the initial temperatures of 900 K and 1100 K does not include the intense reaction rate increase.

2.2.5. Model selection

In a combustion simulation using NODE for chemical reaction calculations, both NODE and the conventional VODE with detailed chemical kinetics are employed. Since NODE is trained based on the auto-ignition calculation results, it is less reliable to predict the reaction rates where the local temperature is below the lowest temperature which is not considered in the zero-dimensional auto-ignition calculation. Therefore, in this method, chemical reaction calculations using NODE are performed at higher temperature regions, and chemical reaction calculations using VODE with detailed chemical kinetics are performed at lower temperature regions. In this study, the threshold used in one- and two-dimensional calculations to select the calculation method either NODE or the conventional VODE with detailed chemical kinetics is determined to be 1400 K, which is higher than the lowest temperature that is contained in the training data. This is because, in the auto-ignition training data whose initial temperature is below 1400 K, the time step interval is significantly large. For instance, static dt in the auto-ignition training data whose initial temperature of 1100 K is in the order of 100 μs. This is significantly larger than the time step interval that is used in one- and two-dimensional calculation, which is in the order of 0.1 μs.

Fig. 2.7 shows an overview of the chemical reaction calculations which utilize NODE at higher temperatures (1400 K and above in this study). When calculating the reaction rate of each chemical species, NODE is branched into three models based on the initial temperature of the training data. This feature not only increases the prediction accuracy due to less generality but the computational costs since the model size can be smaller. In practice, this raises the issues as to which model to use during the chemical reaction calculation. Therefore, it is necessary to decide which model to use in each grid point in advance. Therefore, in this study, in every 100th step during the chemical reaction calculation, the reaction rate of each chemical species is calculated using all three NODEs and the conventional VODE with detailed chemical kinetics. Next, the outputs of NODEs and the reaction rate from VODE are compared, one of the three models of NODEs with the smallest error is selected, and the selected NODE is used for the next 99 steps. This determines the most suitable model to be applied in the chemical reaction calculation among the three models of NODEs. Temperature is calculated iteratively from enthalpy, and the pressure is calculated from the equation of state for ideal gas.

2.2.6. Numerical procedure

All the simulations are performed by using the thermal flow analysis in-house code FK^3 [19] with the finite difference formulation in a non-uniform staggered Cartesian coordinate system. This code is based on a pressure-based semi-implicit solver for compressible flows, which employs a fractional-step method [20,21]. The spatial derivative of the convective term in the conservation equation of momentum is approximated using Kawamura–Kuwahara scheme [22], and the fifth-order WENO (Weighted Essentially Non-Oscillatory) scheme [23] is used to evaluate the convective terms in the conservation equations of the scalar quantities. Time integration of the convective terms is performed by a third-order explicit TVD Runge–Kutta scheme [24].

2.3. Validations

2.3.1. Zero-dimensional calculation

NODE is applied to zero-dimensional auto-ignition calculation to evaluate the evolution of temperature and mass fractions and the ignition delays. The initial conditions are set as 1100 K to 2300 K with 200 K intervals for the temperature and 0.6 to 1.4 with 0.2 intervals for the equivalence ratios. The results are compared with the calculation results obtained by using detailed chemical kinetics with VODE.

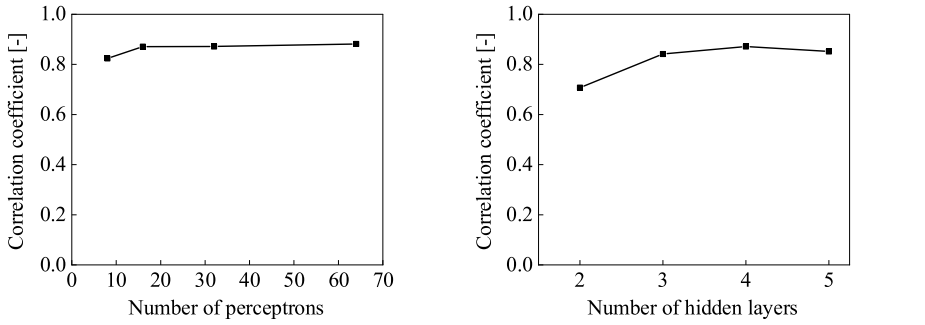

Fig. 2.6. Hyperparameter test for NODE.

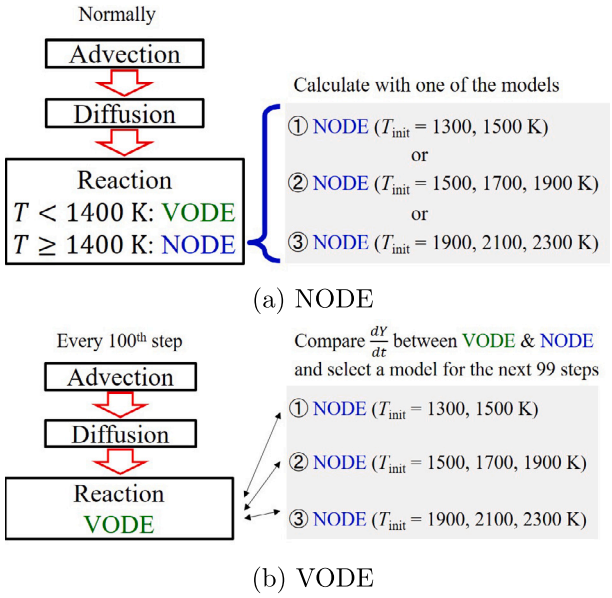

Fig. 2.7. Schematic diagram of chemical reaction calculation procedure in NODE-based calculation.

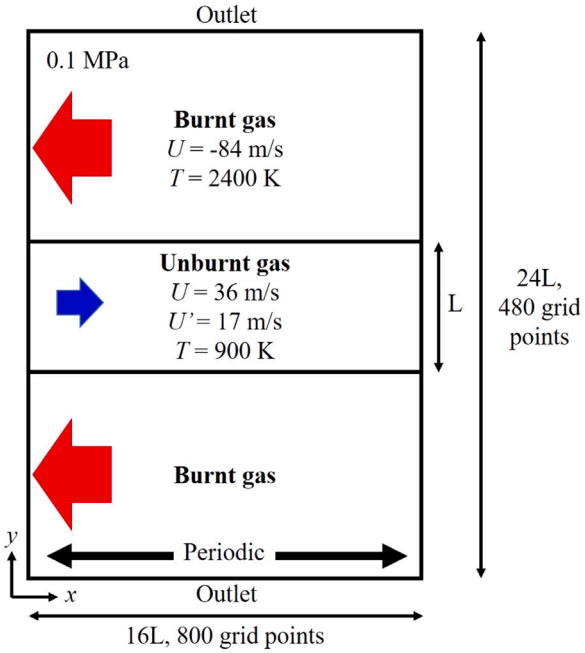

Fig. 2.8. Calculation domain and conditions (L = 1.0 mm).

2.3.2. One-dimensional calculation

NODE is also applied to one-dimensional freely propagating premixed flame for equivalence ratios of 0.8 to 1.2 with 0.1 intervals. The unburnt gas temperature is 300 K, and the ambient pressure is 0.1 MPa. The computational domain measures 20 mm with additional buffer regions on both sides. The minimum grid spacing used is 20 μm. The inlet velocity from the unburnt gas side is determined by the laminar burning velocity to maintain the flame front in the center of the computational domain. The reaction rate calculation using NODE is only used where the local temperature is 1400 K and above, and the conventional VODE with detailed chemical kinetics is used for the remaining region.

2.3.3. Two-dimensional calculation

Fig. 2.8 shows the schematic of the computational domain and conditions for simulating temporary evolving planar jet flame of premixed NH_3. Unburnt gas of the premixed NH_3 and air with an equivalence ratio of 1.0 is set in the center of the domain in y-direction, and burnt gas of the combustion product of the premixed NH_3 and air with an equivalence ratio of 1.0 is set around the unburnt gas. The initial bulk velocities for unburnt and burnt gas are 36 m/s and -84 m/s in x-direction, and both 0 m/s in y-direction. To promote instability and mixing in the boundary between burnt and unburnt gas, artificial velocity fluctuations in x- and y-directions are imposed on the unburnt gas using Klein's digital filter [25], which is 14.2% of the relative velocity of unburnt and burnt gas, 17 m/s. The initial temperatures for unburnt and burnt gas are 900 K and 2400 K. The streamwise boundary condition is periodic, and the other boundaries are outlet conditions. The ambient pressure is 0.1 MPa. The computational domain measures 16 and 24 mm in x- and y-directions respectively and consists of 800 × 480 grid points. The minimum grid spacing used in the DNS grid is 20 μm in each direction, and the grid is stretched at both ends in y-direction.

The CPU time required to simulate temporary evolving planar jet flame of premixed NH_3 using the proposed method is approximately 3000 node hours (about 20 h of real-time) by parallel computing using 7680 cores on the supercomputer Fugaku at RIKEN center, Japan.

3. Results and discussion

3.1. Zero-dimensional calculation

Fig. 3.1 shows the comparison of the temporal profiles of the mass fraction of each species in the zero-dimensional auto-ignition calculation of NH_3/air premixed gas calculated using VODE-based and NODE-based calculation under the initial temperature of 1500 K and

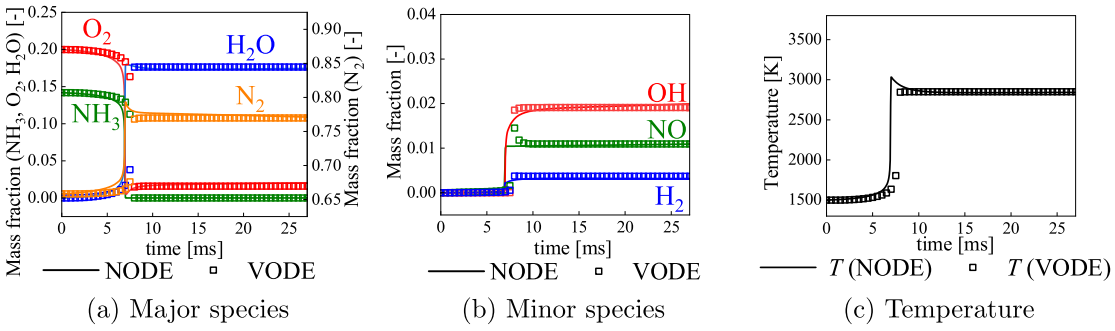

Fig. 3.1. Comparisons of species mass fractions and temperature distribution between VODE-based and NODE-based calculation (ϕ = 1.0, T_{init} = 1500 K).

equivalence ratio of 1.0. This figure shows that the mass fraction of each species can be calculated fairly accurately at 1500 K. Also, the temporal evolution of temperature shows fairly good accuracy, but at the time when the reaction is intense and the mass fraction of the chemical species and temperature changes drastically, NODE-based calculation slightly struggles to follow VODE-based calculation results.

In addition, Figs. 3.2, 3.3, and 3.4 show the comparison of the temporal profiles of the mass fraction of each species for other conditions (T_{init} = 1900 K, ϕ = 0.8, 1.0, 1.2). These show that the mass fraction of each species can also be calculated generally acceptable for wide ranges of conditions, but some discrepancy is noticeable especially for the mass fractions of minor species (NO and OH) as shown in Figs. 3.2(b), 3.3(b), and 3.4(b). It can be seen that for NO and OH, the mass fraction changes even after the ignition. Therefore, even after the major species and temperature has reached an equilibrium state, NODE has to continue predicting the right reaction rates for the intermediate species and these would be consumed to form the final products when achieving complete combustion which requires a longer time. This can be difficult for NODE-based calculation because NODE is required to be sensitive to the small changes in mass fractions and temperature to accurately predict the final stage of the auto-ignition.

Lastly, Figs. 3.5(a) and 3.5(b) show the comparisons of the temporal profiles of the mass fraction of each species for other conditions (T_{init} = 1100 K, ϕ = 0.8). From these figures, mass fractions and temperature before the ignition in the lower initial temperature auto-ignition are also acceptably well reproduced, indicating a reliable prediction of the NODE models for low reaction rates at low temperatures.

The overall discrepancy in the auto-ignition calculation whose initial temperature is 1900 K is more obvious than that of the lower initial temperature case (Fig. 3.1), and it denotes that it is relatively more difficult for NODE-based calculation to predict the reaction rates for higher initial temperature since the reaction is more intense and the reaction rate is increased in higher initial temperatures. However, in terms of the equivalence ratios, the prediction accuracy is almost the same between NODE-based and VODE-based calculations, indicating that the difference in equivalence ratio has little effect on the prediction accuracy of NODE.

Fig. 3.6 shows the comparison of the ignition delay time of NH_3/air premixed flame calculated using VODE-based and NODE-based calculation. The error in the ignition delay time of the initial temperature of 1500 K and above is within 7.5% difference at most. The error slightly increases when the initial temperature is 1300 K and lower since a small error in the low reaction rate region causes a relatively larger discrepancy in ignition delay time compared to the higher initial temperature cases. However, this accuracy is acceptable but not perfect with room to be improved, especially when compared with the deviations between the reduced mechanism predictions and detailed mechanism predictions and experimental data, and the overall prediction of the ignition delay time demonstrates that NODE-based calculation can calculate the ignition delay time for a wide range of initial temperatures and equivalence ratios with reasonable accuracy while reducing the computational costs to 1/24.

The equivalence ratio that is used to train NODE is 0.6 to 1.4 with an interval of 0.2. Therefore, NODE should be able to predict auto-ignition for all the equivalence ratios in Fig. 3.6. The reason NODE slightly over-predicts the ignition delay time for lower equivalence ratios is that when there are thermochemical perturbations at lower equivalence ratios, the thermochemical inputs of NODE can easily step out of the thermochemical states in the training data, hence extrapolation prediction for NODE.

The elementary mass conservation is also investigated in NODE-based calculations. Fig. 3.7 shows the elementary mass conservation of N, H, and O when calculating auto-ignition for the equivalence ratio of 1.0 and initial temperature of 1900 K. This shows that all the elemental mass is well conserved in the entire calculation. However, a slight increase or decrease in mass can be noticed for N and O, which is caused by the unconsidered species in the 52 species in the reaction mechanism. Still, this effect is negligibly small in this case since NODE-based calculations can reproduce the mass fractions of the considered seven species that represent the major component.

The reduction of the computational costs is achieved in aspects of numerical methods and the number of species to consider. Firstly, while VODE employs an implicit time integration method, NODE uses an explicit Euler's method. Since NODE is trained using the auto-ignition calculation results that are calculated by VODE, it is expected to reproduce VODE calculation results with a faster time integration method. Secondly, in VODE calculations, consideration of all the species in the reaction mechanism is required, which invokes a time-consuming iterative loop in the convergence calculation. However, in NODE calculations, the number of species to be considered is reduced, which is an additional advantage in terms of computational costs. An increase in the number of species to be considered will definitely increase the computational costs, which are mainly affected by the threshold value used to identify interested species.

3.2. One-dimensional calculation

Fig. 3.8 shows the instantaneous distribution of the mass fraction of each chemical species and temperature, indicating that most of the mass fractions of chemical species are calculated fairly accurately. However, there are differences between VODE-based and NODE-based calculation in the mass fraction distribution of H_2 and OH as evident from Fig. 3.8(b). This can be attributed to the fact that NODE-based calculation is not capable of predicting the consumption of H_2 and OH in the burnt side with high precision. This error is considered to be caused by that the training data for NODE only consisting of the auto-ignition reaction, and this H_2 and OH consumption in the burnt side does not occur in the auto-ignition.

To further investigate this discrepancy, Fig. 3.9 shows the comparisons of the instantaneous predictions of the H_2 reaction rate obtained

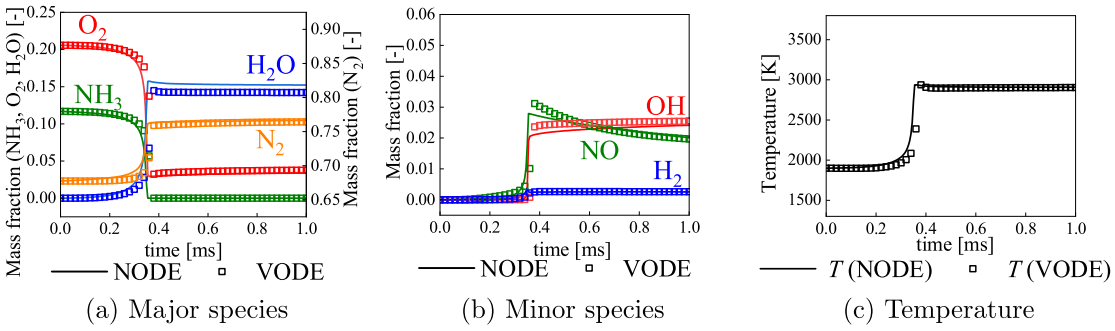

Fig. 3.2. Comparisons of species mass fractions and temperature distribution between VODE-based and NODE-based calculation (ϕ = 0.8, T_{init} = 1900 K).

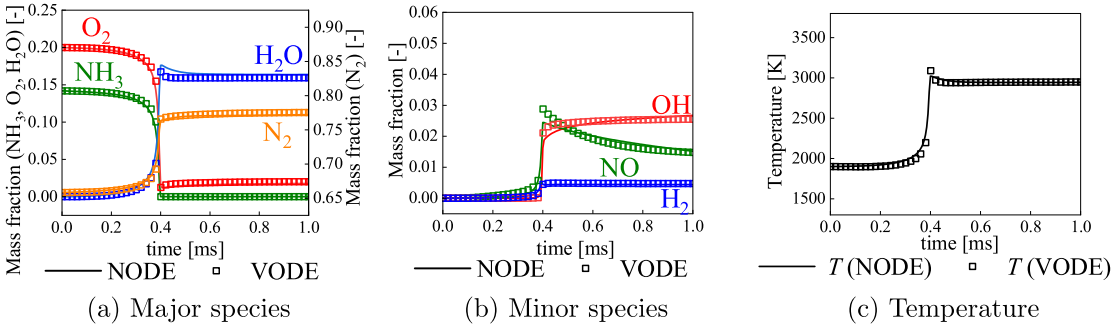

Fig. 3.3. Comparisons of species mass fractions and temperature distribution between VODE-based and NODE-based calculation (ϕ = 1.0, T_{init} = 1900 K).

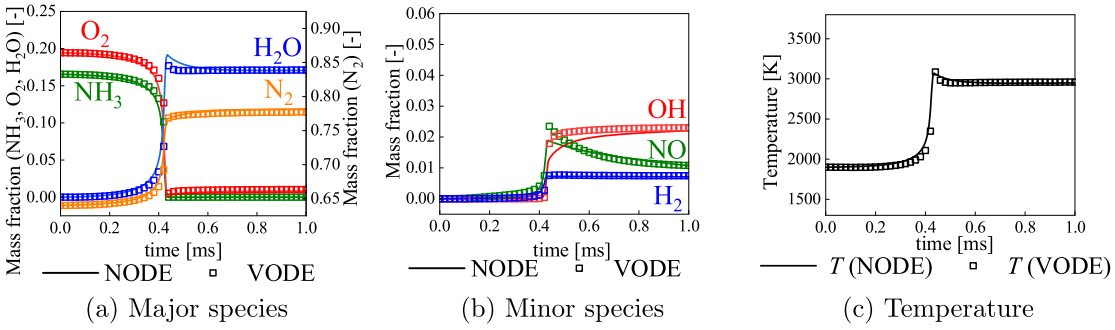

Fig. 3.4. Comparisons of species mass fractions and temperature distribution between VODE-based and NODE-based calculation (ϕ = 1.2, T_{init} = 1900 K).

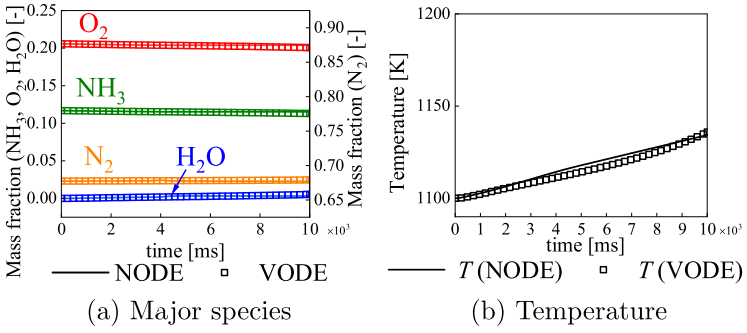

Fig. 3.5. Comparisons of species mass fractions and temperature distribution between VODE-based and NODE-based calculation (ϕ = 0.8, T_{init} = 1100 K).

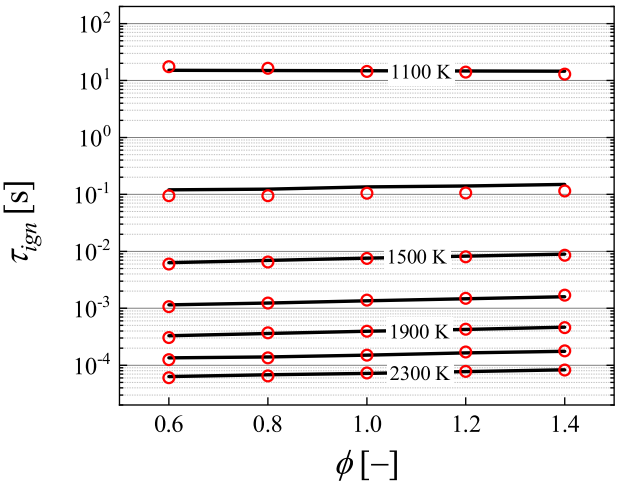

Fig. 3.6. Comparisons of ignition delay time, τ_{ign}, between VODE-based and NODE-based calculation for various initial temperatures, T_{init}, and equivalence ratios, ϕ.

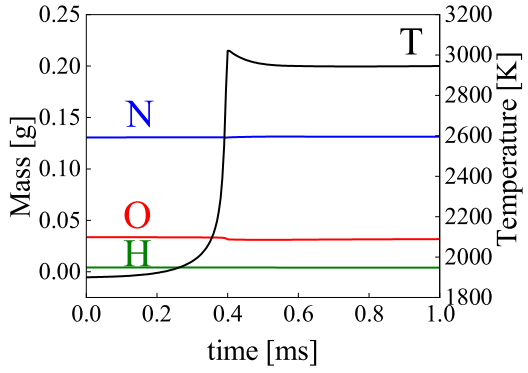

Fig. 3.7. Elemental mass conservation of N, H, and O in NODE-based calculation (ϕ = 1.0, T_{init} = 1900 K).

by VODE and three NODEs branched by the initial temperatures in the training data, which is scheduled at every 100th step in the calculation. As described in Section 2.2.5, model selection is conducted to choose which one of the NODE models to use locally for the next 99 steps in the calculation. Therefore, in this figure, one of the models whose H_2 reaction rate prediction is the closest to that of VODE is chosen for the H reaction rate prediction in the next 99 steps. However, none of the NODE models succeeds in predicting the H_2 reaction rate accurately around where $x = -1$ mm and $x = 0$ mm. At around $x = -1$ mm, none of the NODE models predicts a negative value of the H_2 reaction rate, and at around $x = 0$ mm, all of the NODE models predict less H_2 reaction rate compared with VODE. Therefore, NODE-based calculation fails to reproduce such H_2 production and consumption that is seen in the one-dimensional calculation by VODE-based calculation.

Also, the temperature distribution shows a generally good match between VODE-based calculation and NODE-based calculation. This is due to little difference in the mass fraction distribution of major chemical species, and predominant components of the gas agree sufficiently well with VODE-based calculation.

In addition, Fig. 3.10 shows the laminar burning velocity obtained by using VODE-based and NODE-based calculations. This indicates that NODE-based calculation can calculate the freely-propagating flame fairly well, presumably because the earlier part of the reaction calculation in the unburnt gas is first performed by the conventional VODE-based calculation. Also, NODE-based calculation results in approximately four times faster calculation speed than VODE-based calculation. This improvement in calculation speed is smaller than that in the case of a zero-dimensional auto-ignition reaction, and this is due to the limitation of the calculation time speedup in the region (below 1400 K) where VODE is employed. Therefore, higher computational efficiency can be expected when a wider area of the computational domain has a higher temperature.

3.3. Two-dimensional calculation

Figs. 3.11, 3.12, 3.13, 3.14 show comparisons of mass fraction distribution of NH_3, H_2O, NO, and temperature distribution between the results obtained using VODE-based calculation and those obtained using NODE-based calculation, for the time evolution of the mass fractions of various chemical species in a two-dimensional temporary evolving planar jet flame of premixed NH_3. It is observed that the mass fraction distributions obtained using NODE-based calculation show relatively similar consumption of NH_3 and production of H_2O and NO to those using VODE-based calculation. However, slight over-consumption of the fuel and oxidizer, and over-generation of the product species are also observed, which is further explained as follows.

From Fig. 3.11, the over-consumption of the fuel is apparent with the increase in time. At t = 0.33 ms, even though the mass fraction of NH_3 is high in the VODE-based calculation result around the region circled by the white dotted line, smaller amount of NH_3 is remaining in the NODE-based calculation result. Also, the over-production of the species is noticeable in Fig. 3.12. From this figure, at t = 0.33 ms, some regions where the mass fraction of H_2O is small are observed in the VODE-based calculation result as indicated by the white dotted circle. However, in most of the region, the mass fraction of H_2O is high in the NODE-based calculation result. This over-prediction of the consumption and the production is the accumulation of the error that the predicted reaction rate using NODE has resulted in, which increases the perturbation intensity of the thermochemical states as the inputs to NODEs. In addition, the temperature increase is slightly more intense in the results using NODE-based calculation. This has resulted from the over-prediction of the consumption and production of the mass fraction of species, and the reaction occurs faster in NODE-based calculations than in VODE-based calculations. To amend the problem of the increased perturbation intensity, NODEs are required to be more robust against perturbation of the thermochemical states. Therefore, a more advanced sampling method, such as using 1D flamelet solutions, is required to train NODEs.

Fig. 3.15 shows the comparisons of mass fraction distributions of NH_3 and NO at t = 0.15 ms, each as an example of major and minor species, between the results obtained using VODE-based calculation and those obtained using NODE-based calculation, and white lines indicate where the temperature is 1400 K. The white lines, therefore, denote where the chemical reaction calculation switches to either VODE-based calculation or NODE-based calculation. These figures demonstrate that although the consumption of NH_3 is relatively well reproduced in NODE-based calculations, the production of minor species is globally smaller and locally larger. This represents the same difficulty in calculating the reaction rates for minor species as in one-dimensional calculations.

To further compare the temporal behavior between VODE-based calculation and NODE-based calculation, Fig. 3.16 shows the volume-averaged mass of NH_3 and O_2, and temperature. The volume average is implemented in the region where -0.5 mm $\leq y \leq$ 0.5 mm. From this figure, it can be seen that for the first part of the simulation until t = 0.15 ms, the temporal evolution of each quantity shows similar trends between NODE-based calculation and VODE-based calculation. For the latter part of the calculation from t = 0.15 ms, the discrepancy between NODE-based calculation and VODE-based calculation becomes more noticeable. Judging from the distributions in Figs. 3.11 to 3.14,

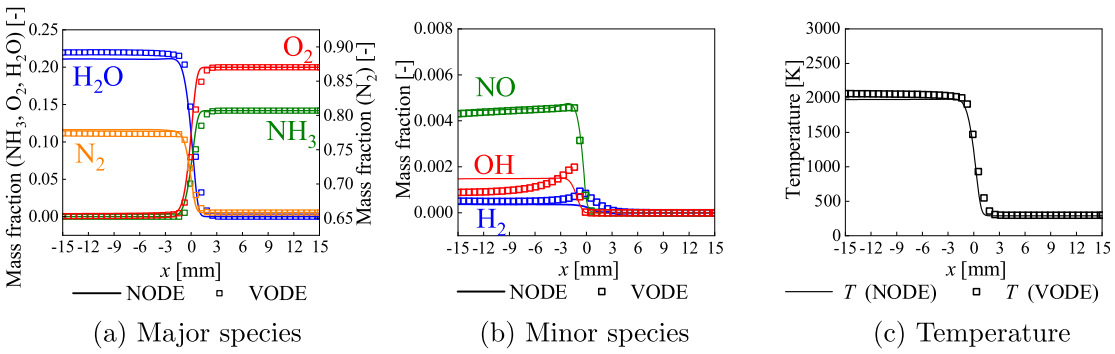

Fig. 3.8. Comparisons of species mass fractions and temperature distribution between VODE-based and NODE-based calculation (ϕ = 1.0).

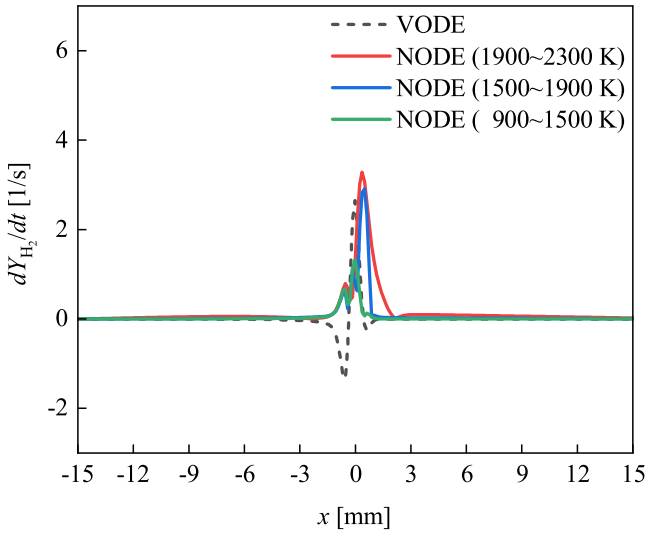

Fig. 3.9. Comparisons of instantaneous predictions of H_2 reaction rate obtained by VODE and three NODEs branched by initial temperatures, T_{init}, in the training data.

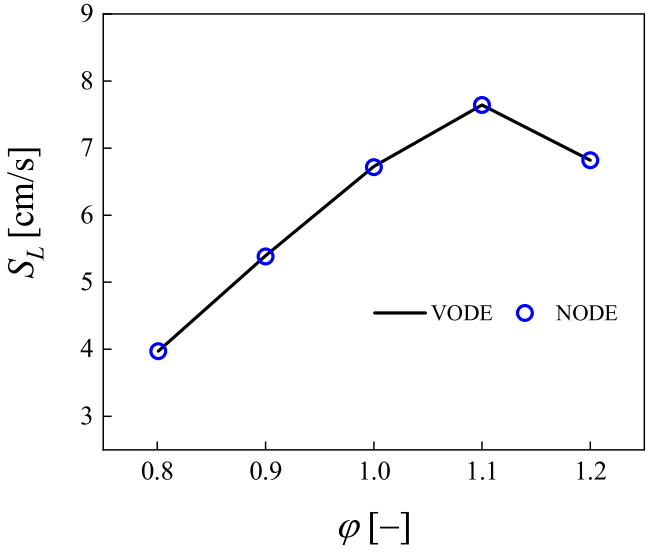

Fig. 3.10. Comparisons of laminar burning velocities, S_L, with equivalence ratio, ϕ, between VODE-based and NODE-based calculation.

after t = 0.15 ms, it can be seen that the mixing of the unburnt gas and burnt gas becomes intense, indicating that the advection and the diffusion of chemical species become drastic. This drastic mixing of the chemical species induces the composition of the gas to be unexpectable for the NODE-based calculation since NODE primarily accounts for the auto-ignition calculation, which leads to the error increase from the VODE-based calculation. As a result, the accumulated error is significant in the temporal evolution of the temperature, since the difference in the composition of the gas increases as time elapses. Further investigation is needed to handle this error accumulation, and one of the solutions is to train NODE with training data not only consisting of the zero-dimensional auto-ignition calculation but other calculations. Since in the more realistic reactions, the chemical compositions can be quite different from those in the auto-ignition calculation. Using one-dimensional calculations such as counter-diffusion flames might be an optimal choice for the additional training data. Also, the computational costs are reduced to 1/38, which is an additional speedup to the one-dimensional calculation. This is because, in NODE-based calculations, the computational costs required to calculate the reaction are constant, whereas in VODE-based calculations, iterative convergence is required and the computational costs increase when the reaction is stiff. Also, NODE-based calculation is faster when a large proportion of the computational domain has a higher local temperature as NODE can be applied in a wider region in the reaction calculation instead of VODE. In the two-dimensional calculation, the lowest temperature is 900 K and it is higher than that in the one-dimensional calculation, which is 300 K.

4. Conclusions

In this study, NODE-based calculation was applied to conduct NH_3 combustion simulations, and the accuracy and computational cost of this method were verified by comparing them with VODE-based calculation via ignition delay time, laminar combustion velocity, distributions of temperature and mass fraction of each chemical species, and computational costs.

In the zero-dimensional auto-ignition calculations, it was observed that this method was able to reproduce the temporal evolution of the mass fraction of species and temperature, as well as the ignition delay time for a wide range of initial temperatures and equivalence ratios fairly accurately with the calculation cost reduced to 1/24 compared with VODE-based calculation. On the other hand, for the distribution of the mass fraction of each chemical species after ignition, slight differences were observed compared with the results of VODE-based calculation, and this was caused by the NODE prediction error in the reaction rate calculation where the reaction was intense. This tendency was more obvious when the initial temperature was high, which induced more stiffness in the reaction calculation, but not relevant to the change in the equivalence ratios.

In the one-dimensional freely propagating flame calculations, NODE-based calculation was able to reproduce the one-dimensional

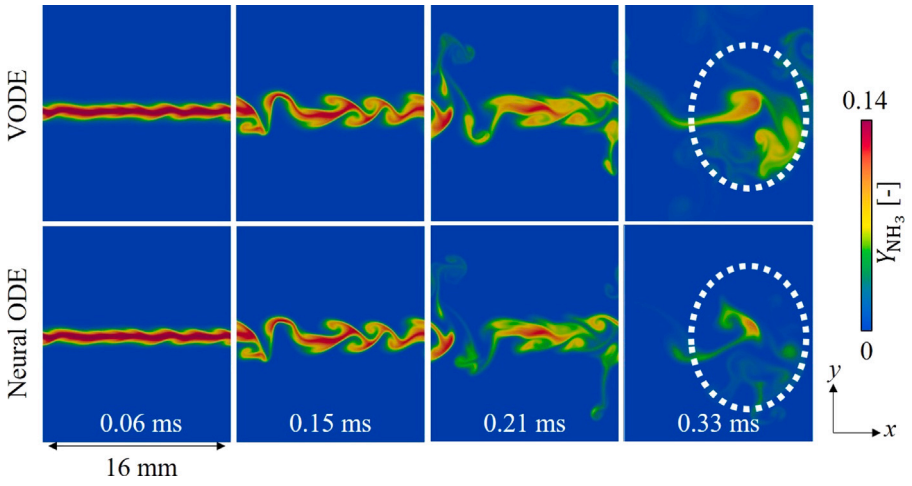

Fig. 3.11. Comparisons of mass fraction distribution of NH_3 between VODE-based and NODE-based calculation.

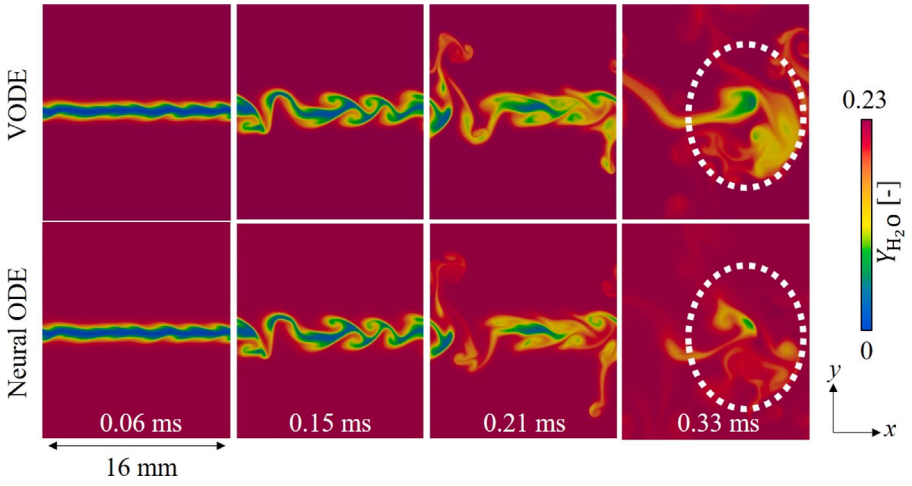

Fig. 3.12. Comparisons of mass fraction distribution of H_2O between VODE-based and NODE-based calculation.

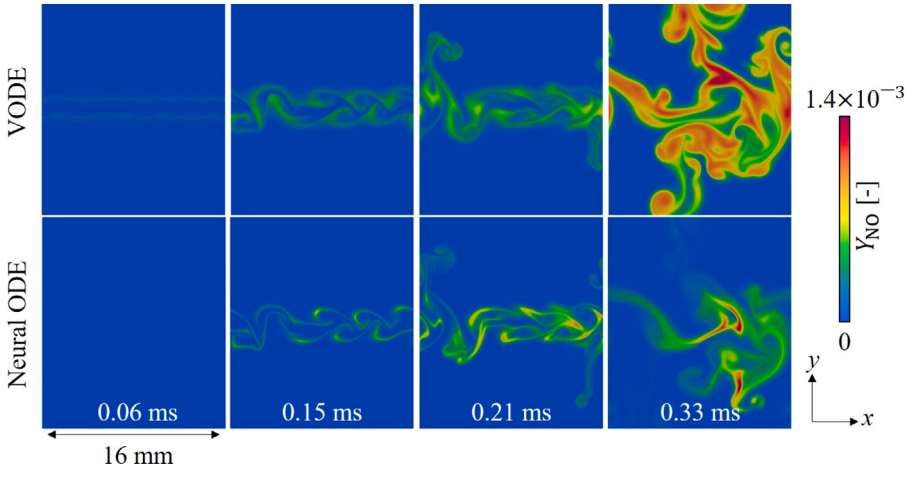

Fig. 3.13. Comparisons of mass fraction distribution of NO between VODE-based and NODE-based calculation.

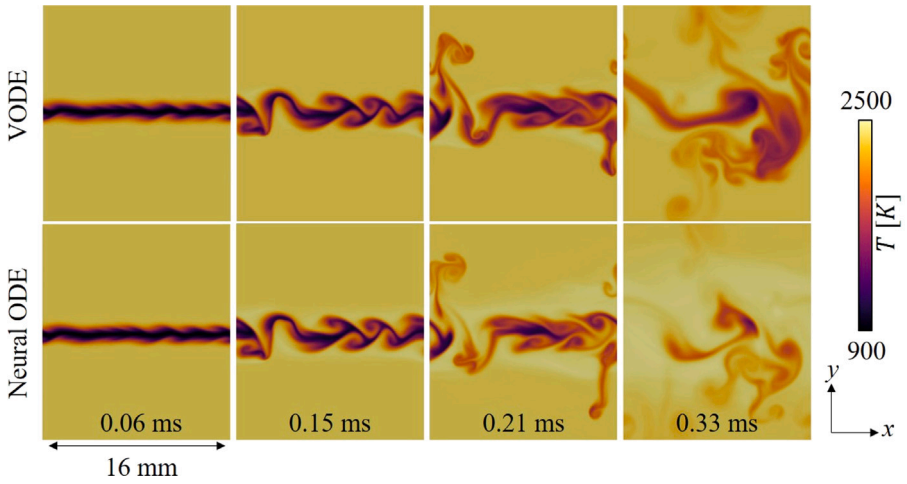

Fig. 3.14. Comparisons of temperature distribution between VODE-based and NODE-based calculation.

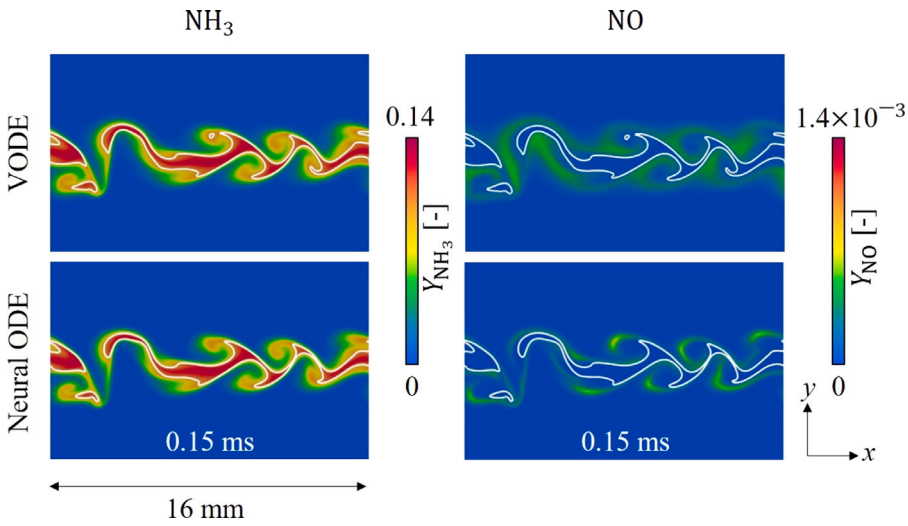

Fig. 3.15. Comparisons of mass fraction distribution of NH_3 and NO between VODE-based and NODE-based calculation (white lines indicate T = 1400 K).

distribution of the mass fraction of each chemical species and temperature fairly accurately while reducing the calculation cost to 1/4 compared with VODE-based calculation. However, the distribution of the mass fraction of each chemical species and temperature obtained using NODE-based calculation had some discrepancies in the burnt side of the profile compared with that of VODE-based calculation. This is due to the low prediction accuracy of the reaction rate of minor species, especially OH and H_2 since the behavior of production and consumption as an intermediate product is different in the one-dimensional calculations from that of the zero-dimensional calculations.

In the two-dimensional jet flame calculation, NODE-based calculation was able to reproduce the distribution of mass fractions of chemical species and temperature relatively accurately with a calculation cost reduced to 1/38 compared with the VODE-based calculation. On the other hand, overconsumption of the fuel and oxidizer and overproduction of species were observed. This was similar to the results obtained in one-dimensional calculations that the behavior of production and consumption of the species that was ought to be occurring in the multi-dimensional calculations were not included in the training data for NODE, but only zero-dimensional auto-ignition calculations were taken into account.

Future work is to improve NODE-based calculations with additional training data and investigate the versatility of this method to other conditions such as different fuels and pressure.

Declaration of competing interest

The authors declare that they have no known competing financial interests or personal relationships that could have appeared to influence the work reported in this paper.

Code availability

Codes for training NODEs are publicly available at https://github.com/saitomanabu/AmmoniaNODE.

Data availability

Data will be made available on request.

Acknowledgments

The authors would like to thank Mr. Shuto Kawaguchi, who was a member of our laboratory team, for useful discussions. This work was partially supported by MEXT, Japan as “Program for Promoting Researches on the Supercomputer Fugaku” (Development of the Smart design system on the supercomputer “Fugaku” in the era of Society 5.0) (JPMXP1020210316). This research used the computational resources of supercomputer Fugaku provided by the RIKEN Center for Computational Science (Project ID: hp220180).

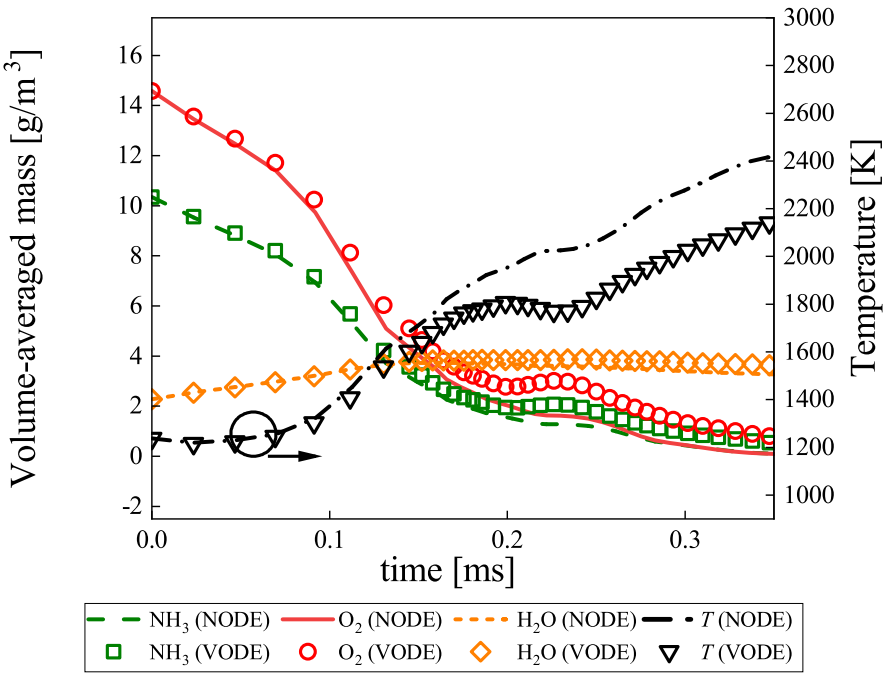

Fig. 3.16. Comparisons of volume-averaged mass and temperature between VODE-based and NODE-based calculation.

References

[1] Lu T, Law CK. Toward accommodating realistic fuel chemistry in large-scale computations. Prog Energy Combust Sci 2009;35(2):192–215.

[2] Ó Conaire M, Curran HJ, Simmie JM, Pitz WJ, Westbrook CK. A comprehensive modeling study of hydrogen oxidation. Int J Chem Kinetics 2004;36(11):603–22.

[3] Kobayashi H, Hayakawa A, Somarathne KKA, Okafor EC. Science and technology of ammonia combustion. Proc Combust Inst 2019;37(1):109–33.

[4] Smith GP. GRI-mech 3.0. 1999, http://www.me.berkley.edu/gri_mech/.

[5] Schwer DA, Lu P, Green Jr WH. An adaptive chemistry approach to modeling complex kinetics in reacting flows. Combust Flame 2003;133(4):451–65.

[6] Van Oijen J, De Goey L. Modelling of premixed laminar flames using flamelet-generated manifolds. Combust Sci Technol 2000;161(1):113–37.

[7] Kasuya H, Iwai Y, Itoh M, Morisawa Y, Nishiie T, Kai R, Kurose R. LES/flamelet/ANN of oxy-fuel combustion for a supercritical CO2 power cycle. Appl Energy Combust Sci 2022;12:100083.

[8] Ihme M, Schmitt C, Pitsch H. Optimal artificial neural networks and tabulation methods for chemistry representation in LES of a bluff-body swirl-stabilized flame. Proc Combust Inst 2009;32(1):1527–35.

[9] Honzawa T, Kai R, Hori K, Seino M, Nishiie T, Kurose R. Experimental and numerical study of water sprayed turbulent combustion: Proposal of a neural network modeling for five-dimensional flamelet approach. Energy AI 2021;5:100076.

[10] Zhang T, Yi Y, Xu Y, Chen ZX, Zhang Y, Weinan E, Xu Z-QJ. A multi-scale sampling method for accurate and robust deep neural network to predict combustion chemical kinetics. Combust Flame 2022;245:112319.

[11] Wan K, Barnaud C, Vervisch L, Domingo P. Chemistry reduction using machine learning trained from non-premixed micro-mixing modeling: Application to DNS of a syngas turbulent oxy-flame with side-wall effects. Combust Flame 2020;220:119–29.

[12] Chen RT, Rubanova Y, Bettencourt J, Duvenaud DK. Neural ordinary differential equations. Adv Neural Inf Process Syst 2018;31.

[13] Owoyele O, Pal P. ChemNODE: A neural ordinary differential equations framework for efficient chemical kinetic solvers. Energy AI 2022;7:100118.

[14] Okafor EC, Naito Y, Colson S, Ichikawa A, Kudo T, Hayakawa A, Kobayashi H. Experimental and numerical study of the laminar burning velocity of CH4–NH3–air premixed flames. Combust Flame 2018;187:185–98.

[15] Goodwin DG, Moffat HK, Schoegl I, Speth RL, Weber BW. Cantera: An object-oriented software toolkit for chemical kinetics, thermodynamics, and transport processes. 2022, http://dx.doi.org/10.5281/zenodo.6387882, Version 2.6.0. https://www.cantera.org.

[16] Brown PN, Byrne GD, Hindmarsh AC. VODE: A variable-coefficient ODE solver. SIAM J Sci Statist Comput 1989;10(5):1038–51.

[17] Box GE, Cox DR. An analysis of transformations. J R Stat Soc Ser B Stat Methodol 1964;26(2):211–43.

[18] Elfwing S, Uchibe E, Doya K. Sigmoid-weighted linear units for neural network function approximation in reinforcement learning. Neural Netw 2018;107:3–11.

[19] About in-house code FK^3. 2023, http://www.tse.me.kyoto-u.ac.jp/members/kurose/link.php, (visited on 3/13/23).

[20] Moureau V, Bérat C, Pitsch H. An efficient semi-implicit compressible solver for large-eddy simulations. J Comput Phys 2007;226(2):1256–70.

[21] Kai R, Masuda R, Ikedo T, Kurose R. Conjugate heat transfer analysis of methane/air premixed flame–wall interaction: A study on effect of wall material. Appl Therm Eng 2020;181:115947.

[22] Kawamura T, Kuwahara K. Computation of high Reynolds number flow around a circular cylinder with surface roughness. In: 22nd Aerospace Sciences Meeting. 1984, p. 340.

[23] Jiang G-S, Shu C-W. Efficient implementation of weighted ENO schemes. J Comput Phys 1996;126(1):202–28.

[24] Gottlieb S, Shu C-W. Total variation diminishing Runge-Kutta schemes. Math Comput 1998;67(221):73–85.

[25] Klein M, Sadiki A, Janicka J. A digital filter based generation of inflow data for spatially developing direct numerical or large eddy simulations. J Comput Phys 2003;186(2):652–65.